Hindawi Publishing Corporation
Journal of Nanotechnology
Volume 2012, Article ID 712850, 8 pages
doi:10.1155/2012/712850

Research Article

Synthesis of 1D, 2D, and 3D ZnO Polycrystalline Nanostructures Using the Sol-Gel Method

Yung-Kuan Tseng,[1,2] Ming-Hung Chuang,[2] Yen-Cheng Chen,[2] and Chao-Hsien Wu[2]

[1] *Department of Cultural Heritage Conservation, National Yunlin University of Science and Technology, Douliou 64002, Taiwan*
[2] *Graduate School of Materials Science, National Yunlin University of Science and Technology, Douliou 64002, Taiwan*

Correspondence should be addressed to Yung-Kuan Tseng, kuan@yuntech.edu.tw

Received 4 December 2011; Accepted 25 February 2012

Academic Editor: Yahya A. Ismail

This study employed various polyol solvents to synthesize zinc oxide polycrystalline nanostructures in the form of fibers (1D), rhombic flakes (2D), and spheres (3D). The synthetic process primarily involved the use of zinc acetate dihydrate in polyol solutions, which were used to derive precursors of zinc alkoxides. Following hydrolysis at 160°C, the zinc alkoxide particles self-assembled into polycrystalline nanostructures with different morphologies. Following calcination at 500°C for 1 h, polycrystalline ZnO with good crystallinity was obtained. FE-SEM explored variations in surface morphology; XRD was used to analyze the crystalline structures and crystallinity of the products, which were confirmed as ZnO wurtzite structures. FE-TEM verified that the ZnO nanostructures were polycrystalline. Furthermore, we employed TGA/DSC to observe the phase transition. According to the results of property analyses, we proposed models of the relevant formation mechanisms. Finally, various ZnO structures were applied in the degradation of methylene blue to compare their photocatalytic efficiency.

1. Introduction

In recent years, zinc oxide (ZnO) has become the subject of much research due to its excellent attributes as an II–VI semiconductor [1, 2]. At room temperature, it possesses a wide direct band gap (3.37 eV) as well as a high exciton binding energy of approximately 60 meV [3]. By contrast, the free exciton binding energy of GaN is only 26 meV. Greater exciton binding energy enhances the light emission efficiency of excitons at room temperature [4], the mechanism of which can be applied in photoelectric conversion components, solar cells, UV lasers, piezoelectric and thermoelectric materials, nanometer photocatalysts, and gas sensors. Furthermore, ZnO has high thermal stability and UV absorption but does not absorb visible light, enabling its use in transparent conductive components. As well as titanium dioxide, ZnO is also an effective photocatalyst.

The application of ZnO nanostructures in nanodevices has attracted considerable attention in the last few years, leading to studies on various forms of syntheses. For example, many studies have conducted cylindrical, linear, and tubular forms of one-dimensional syntheses [5–9]; research on two-dimensional nanostructures is relatively rare [10–13]; more complex three-dimensional nanostructures are composed of low-dimensional nanostructures [14, 15].

Currently, there are many methods to fabricate ZnO nanostructures or microstructures. Oxidation of zinc vapor [16] involves placing metal zinc powder into a crucible and heating it in a furnace; at 419.53°C, the powder melts into liquid state before evaporating into zinc vapor. Oxygen is introduced to react with the zinc vapor and form needle-shaped crystal whiskers of ZnO. Chemical vapor deposition (CVD) [17] is another approach that utilizes energy sources such as heat, plasma discharge, or UV irradiation to enable chemical reactions of vapor substances on the heated surface of a solid, where the stable solid products of the reaction are deposited. The vapor-liquid-solid method (VLS) [18, 19] is the most common process for the fabrication of ZnO nanostructures. High temperatures are required to vaporize or decompose ZnO growth sources; a catalyst and the resulting zinc vapor then produce an alloy with a low melting point. Zinc precipitates from the supersaturated

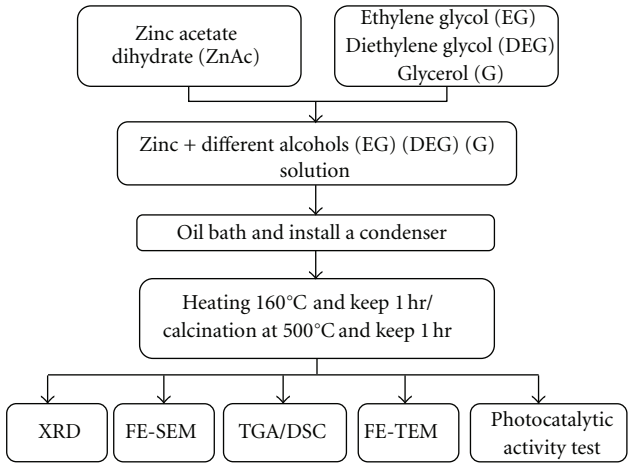

Figure 1: Procedure of the experiment.

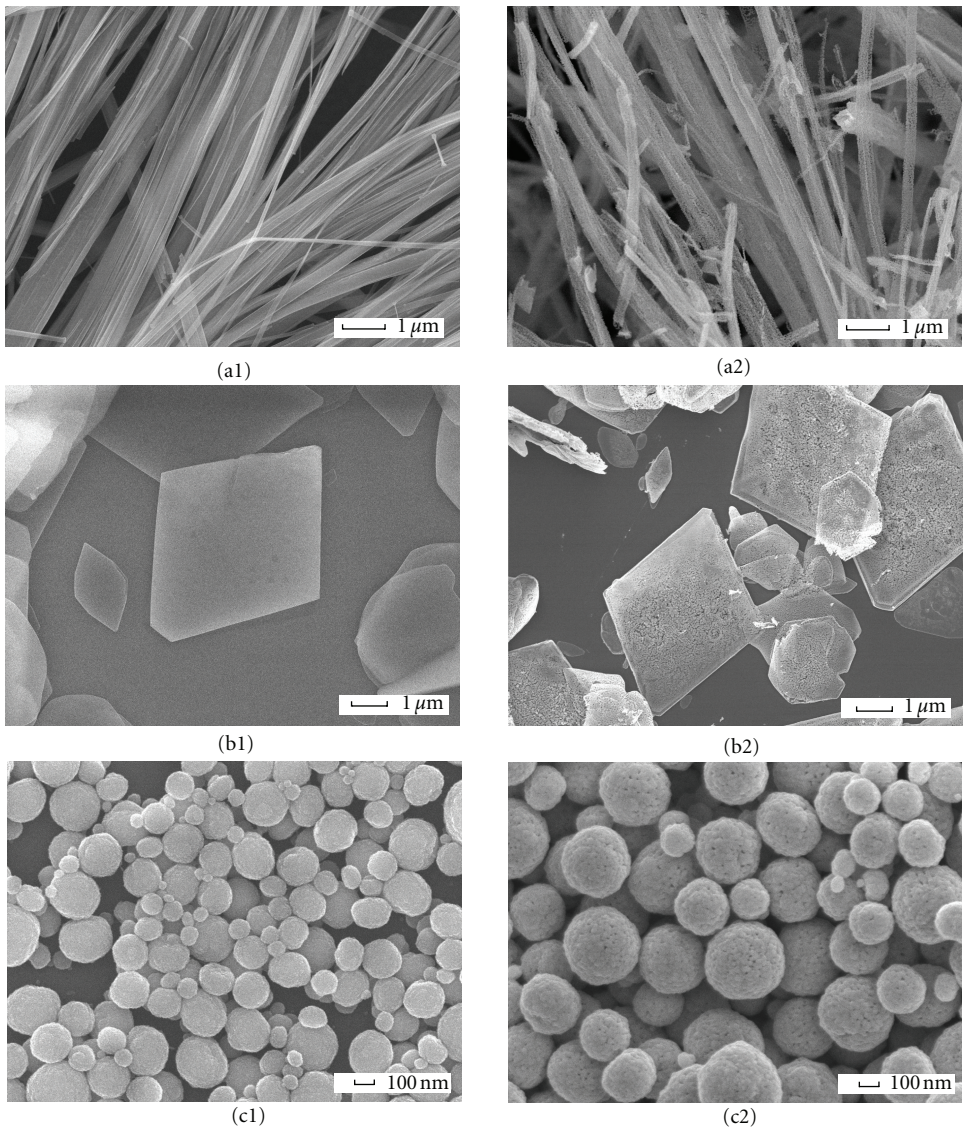

Figure 2: Various surface morphologies of synthesized ZnO: (a1), (b1), and (c1) ZnO gel solutions dried at 160°C; (a2), (b2), and (c2) samples calcinated at 500°C.

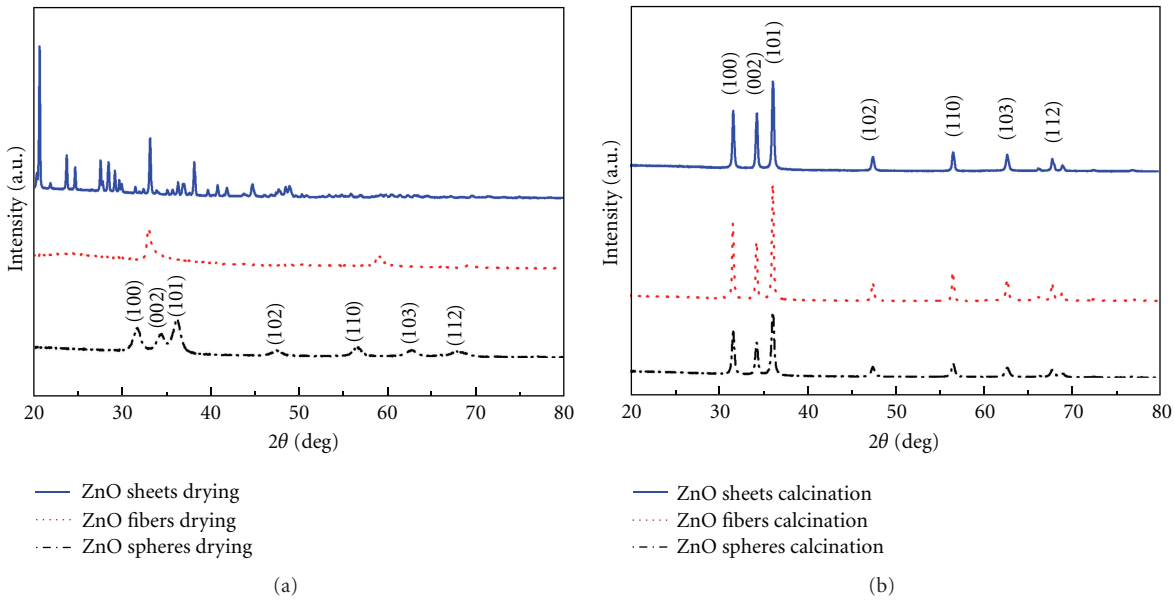

Figure 3: XRD graphs of ZnO fibers, ZnO spheres, and ZnO flakes following (a) drying at 160°C and (b) calcination at 500°C.

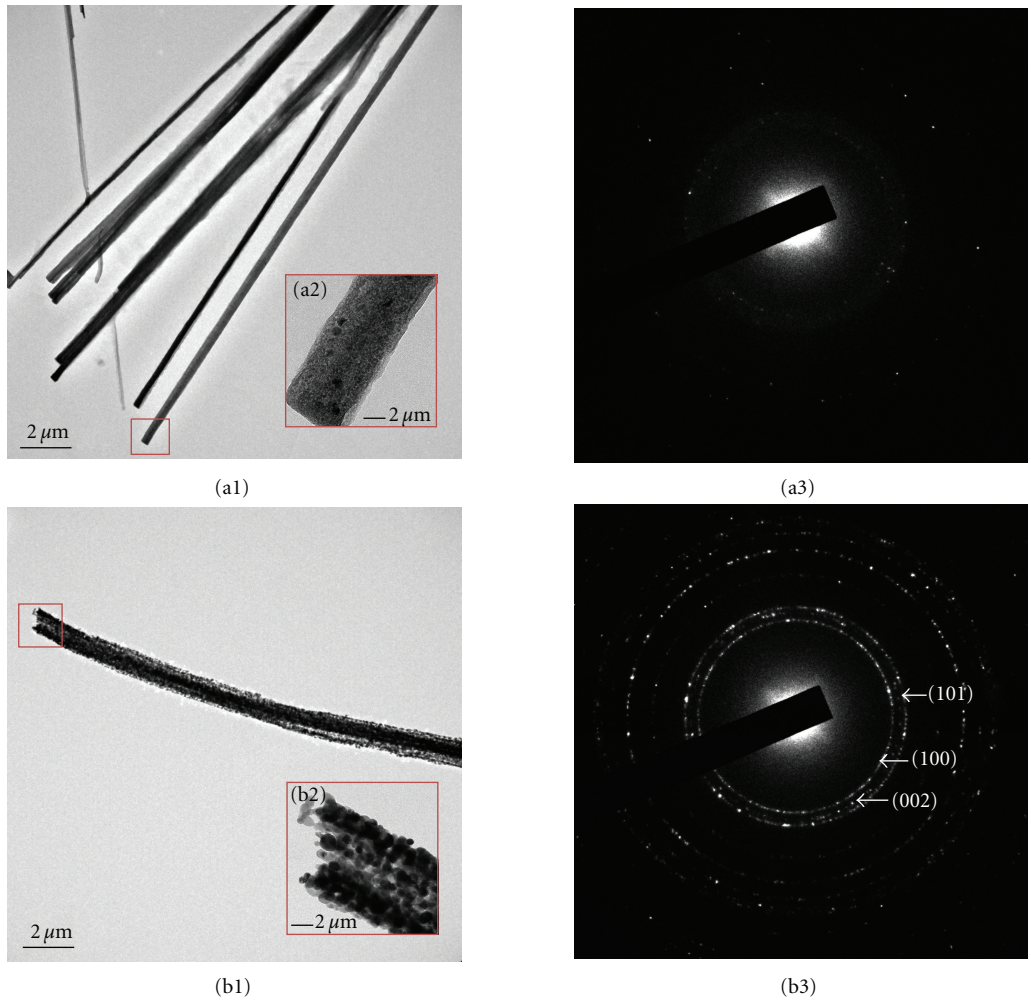

Figure 4: SAED graphs and FE-TEM images of ZnO fibers: (a1), (a2), and (a3) samples dried at 160°C; (b1), (b2), and (b3) samples calcinated at 500°C.

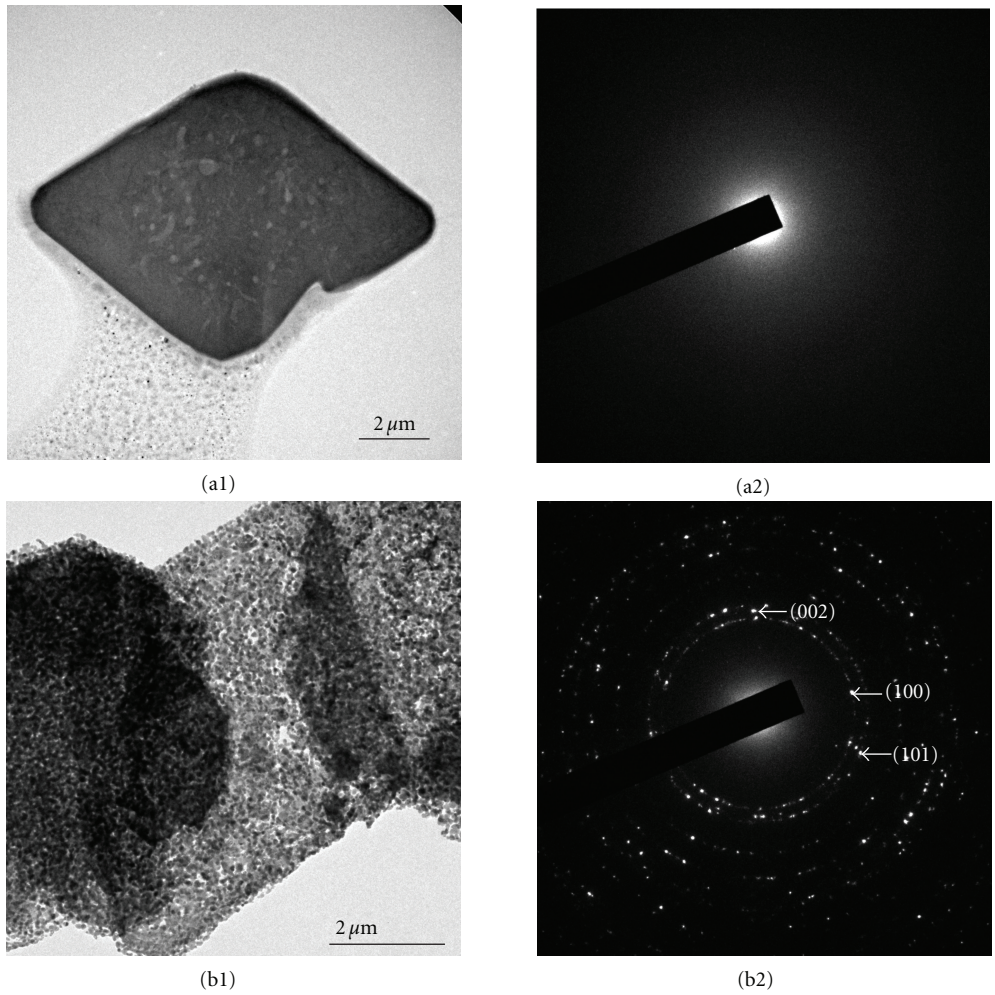

Figure 5: SAED graphs and FE-TEM images of ZnO flakes: (a1) and (a2) samples dried at 160°C; (b1) and (b2) samples calcinated at 500°C.

alloy before merging with atmospheric oxygen to form ZnO nanowires. The ZnO nanowires synthesized via the VLS method are generally monocrystalline, the diameter of which is determined by the particle size of the catalyst. Finally, the template-based method [20] employs methods such as electroplating, CVD, and the sol-gel method to grow the desired substance in the holes of a porous alumina substrate, the growth template. The ZnO nanostructures obtained from this method are polycrystalline.

Regardless of monocrystalline or polycrystalline results, most methods for producing ZnO structures require high temperatures or high costs. This study proposes a low-cost sol-gel method to fabricate various forms of ZnO structures. This novel process is fast and can be completed at lower temperatures. Moreover, the photocatalytic effect of the fiber ZnO structures produced with ethylene glycol as the solvent is superior to that of commercial ZnO.

2. Experiment Methods

2.1. Synthesis. All of the chemicals employed in this study were of analytical grade and required no further purification. This study employed three alcohols as solvents in the sol-gel method to fabricate various ZnO nanostructures: ethylene glycol (EG), glycerol (G), and diethylene glycol (DEG). The structural, physical, and optical properties of the ZnO products generated from the three solvents were compared.

The synthesis was divided into three processes: solution preparation, heating to promote hydrolysis, and heat treatment of the products.

The steps involved in the synthesis are as follows.

(1) 0.1 M of zinc acetate dihydrate ($Zn(CH_3COO)_2 \cdot 2H_2O$) is placed in a 250 mL round-bottom flask.

(2) 100 mL of the solvent (EG, G, or DEG) is added to the flask.

(3) The round-bottom flask is equipped with a reflux apparatus and placed in an oil bath, where the solution is heated and stirred.

(4) The solution is heated at a rate of 1°C/min. When the temperature approaches 160°C, the clear solution becomes milky white. The temperature of the solution is maintained at 160°C for 1 h.

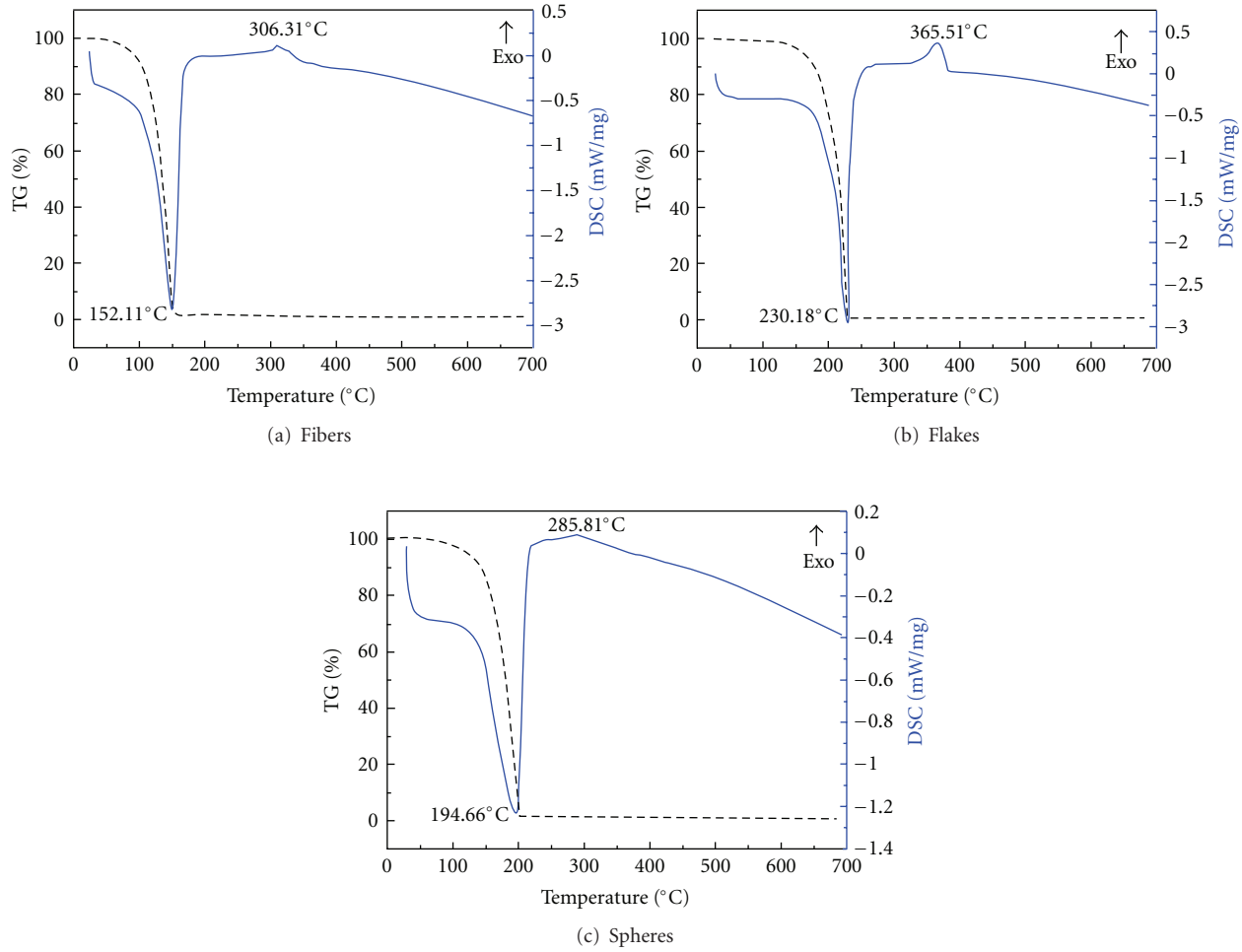

Figure 6: TGA/DSC graphs of the precursor of various ZnO structures: (a) fibers, (b) flakes, and (c) spheres.

(5) The milky white solution is dripped onto silicon substrates and dried on a hot plate at 160°C, forming one sample type. For the other sample type, the solution is placed in a high-temperature furnace and heated to 500°C at a rate of 5°C/min under atmospheric conditions. The temperature is maintained for 1 h, and the sample is taken out once its temperature cools to room temperature.

The experimental procedure is illustrated in Figure 1.

2.2. Property Analysis. Field emission scanning electron microscopy (FE-SEM, JEOL JSM7500F) was performed on the sample dried at 160°C and the sample calcinated at 500°C to explore their surface morphology. High-resolution X-ray diffraction (HR-XRD, PHILIPS X'PERT Pro MPD) was employed to analyze the structural properties of the samples, and the phase transition during the synthetic process was observed using simultaneous thermogravimetric analyzer and differential scanning calorimeter (TGA/DSC, TA Instruments-SDT 2960). A field emission transmission electron microscope (FE-TEM JEOL JEM-2100F) was used to observe the appearance and crystalline structure.

2.3. Photocatalytic Activity Test. Three different morphologies of synthesized ZnO were compared with commercial ZnO. Samples were placed in methylene blue solutions and exposed to UV-C light for an hour. The absorption values of the samples were measured every 20 min using UV-visible spectroscopy (JASCO V-630).

3. Results and Discussion

3.1. Surface Morphology. From FE-SEM observations, this study determined that the application of zinc acetate dihydrate as a solute in conjunction with EG, G, and DEG as solvents in sol-gel reactions enables the formation of ZnO with varying morphologies. Figure 2 presents the various types of ZnO that can be obtained from ZnAc with various polyols and heat treatments. Using EG, G, and DEG as the solvents resulted in fiber structures (Figures 2(a1) and 2(a2)), flake structures (Figures 2(b1) and 2(b2)), and spherical structures (Figures 2(c1) and 2(c2)), respectively. All of the samples with gel solutions synthesized at 160°C and then dried on a hot plate at 160°C presented a smooth micromorphology (Figures 2(a1), 2(b1), and 2(c1)). The samples

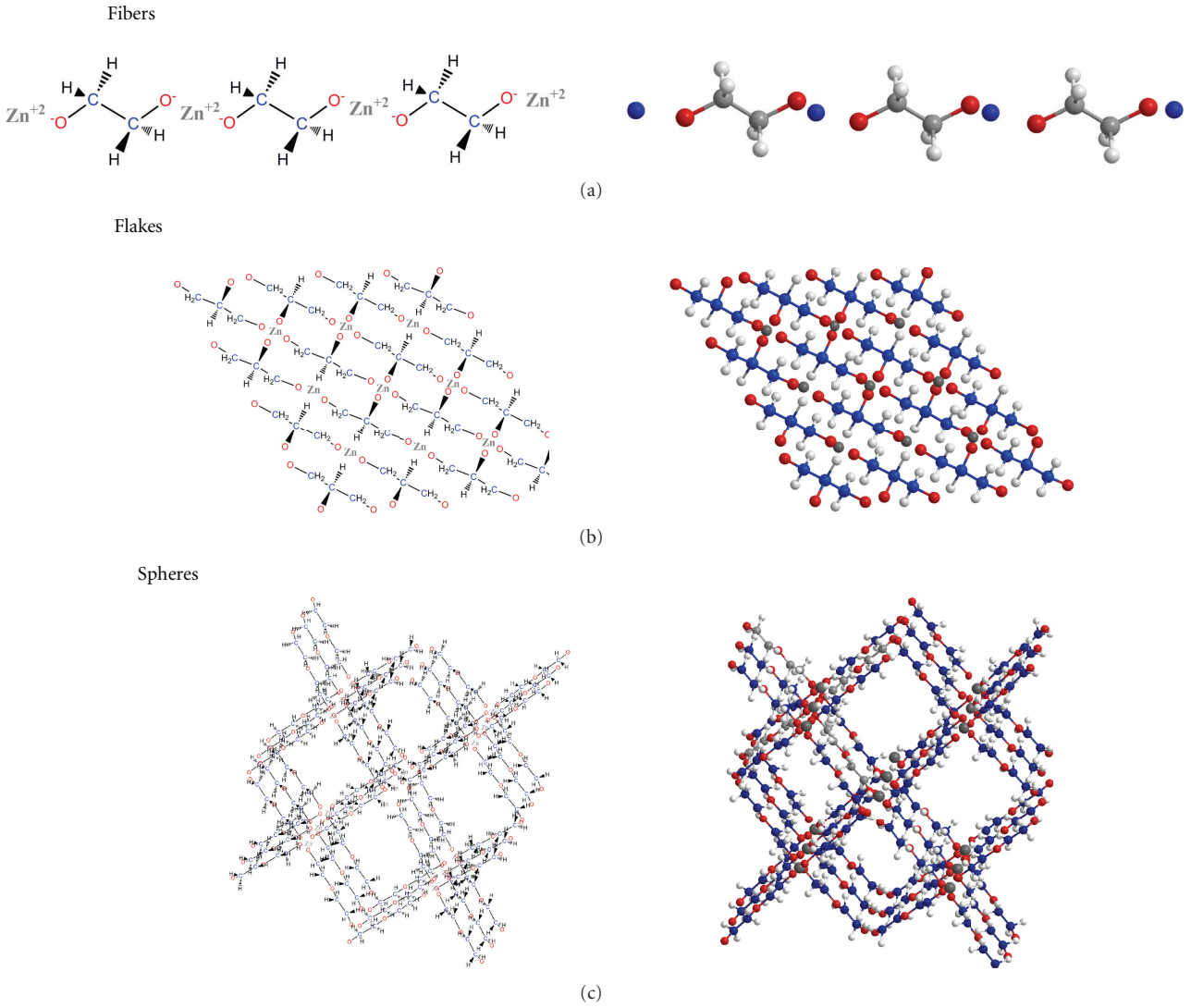

Figure 7: Formation mechanisms of ZnO fibers (1D), ZnO flakes (2D), and ZnO spheres (3D). Color code: blue: carbon, white: hydrogen, red: oxygen, and grey: zinc.

calcinated in air at 500°C remained unchanged in shape but exhibited rougher surfaces with additional holes and cracks (Figures 2(a2), 2(b2), and 2(c2)), which were due to the conversion of the larger zinc alkoxide particles into the smaller ZnO crystals.

3.2. Structural Properties. Figure 3 shows the XRD graphs of the three types of zinc compound dried at 160°C and calcinated at 500°C. The graphs of the samples dried at 160°C were compared with JCPDS files, of which no files were found to be identical to the ZnO flakes and fibers. No similar graphs were found in the literature either. We speculate that the two XRD graphs are consistent with the crystal structure of zinc alkoxides. The spherical structures dried at 160°C are consistent with ZnO structures, as shown in Figure 3(a). This indicates that using DEG as the solvent can hydrolyze ZnAc into ZnO at lower temperatures. Regarding the three samples calcinated at 500°C, the XRD graphs were recognized as identical to nos. 36-1451 in the JCPDS files, namely, wurtzite structures (Figure 3(b)).

Figure 4 shows the appearance and crystalline structure of the zinc compounds observed by FE-TEM. Figure 4(a1) shows the ZnO fibers synthesized at 160°C; Figure 4(a2) is a partial enlargement of Figure 4(a1). Figure 4(a3) is the selected area electron diffraction (SAED) graph of the ZnO fibers; some crystals, speculated as ZnO fiber structures, are already apparent. Figure 4(b1) is an image of the ZnO fibers calcinated at 500°C; Figure 4(b2) is a partial enlargement of Figure 4(b1). Figure 4(b3) exhibits the SAED graph following calcinations, revealing superior crystallinity to that in Figure 4(a3). Figures 5(a1) and 5(a2) are the SAED graphs of the ZnO flakes synthesized at 160°C, and Figures 5(b1) and 5(b2) are the SAED graphs of the calcinated ZnO flakes. Figures 4 and 5 demonstrate that the number of holes and cracks increases when zinc alkoxide turns into ZnO during calcination. Moreover, the crystallinity improves, and

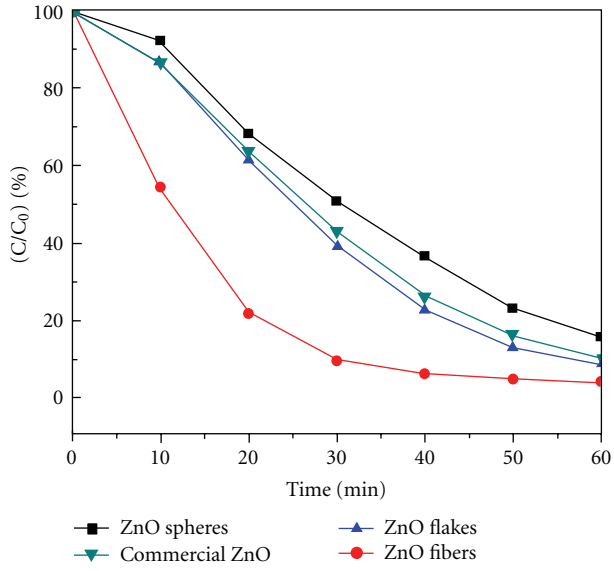

FIGURE 8: Comparison of photocatalytic effects of various ZnO structures.

polycrystalline structures form, which correspond with the XDR graphs.

The precursor solutions of the three different morphologies of ZnO were further analyzed by TGA/DSC to investigate the influence of the heat treatment on the samples. Figure 6 presents the results of the TGA/DSC analysis. Each sample exhibited a distinct endothermic peak followed by a marked loss in weight at the lower temperatures of 152.11°C, 230.18°C, and 194.66°C, respectively. The endothermic peaks and weight loss are primarily caused by the vaporization of the alcohols in the solution, leaving zinc alkoxide behind. Furthermore, the three different surface morphologies of ZnO showed exothermic peaks at 306.31°C, 365.51°C, and 285.81°C, respectively, indicating the pyrolysis of zinc alkoxide and the energy required for it to sinter into ZnO. As seen in Figure 6, spherical structures require the least amount of energy to be converted into ZnO, thereby explaining the reason why the spherical sample is capable of forming crystalline ZnO structures at a lower temperature.

3.3. Formation Mechanism. Due to the heating, the ZnAc within the solution undergoes hydrolysis forming acetate ions and zinc ions. With the abundance of electrons in the oxygen atoms, the hydroxyl groups (–OH) of alcohol molecules bond with the zinc ions. The resulting alkoxides are such as shown in (1)–(3). Figure 7 presents the bonding processes for ZnO fiber structures, sheet structures, and spherical structures. When using EG as the solvent, the two sides of the zinc ions form ionic bonds with the oxygen ions, which link to more ions and form long fiber-like structures (Figure 7(a)).

With G as the solvent, the glycerol possesses three hydroxyl groups that can react with the zinc ions. Because the electronic configuration of the zinc ions is $[Ar]3d^{10}$, 4s and 4p merge into an empty sp^3 orbital, which further forms coordinate covalent bonds with the oxygen ions in the alkoxy groups created by the glycerol. Under the conditions enabling the formation of coordinate covalent bonds with minimal three-dimensional obstacles, simulation showed the resulting sheet structures exhibited in (Figure 7(b)).

The reaction principles under the circumstances with DEG as the solvent are similar to those with glycerol. Due to the longer molecular structures of DEG and in consideration of conditions enabling the formation of coordinate covalent bonds with minimal three-dimensional obstacles, 3D structures are more probable (Figure 7(c)). These 3D structures form sphere colloid particles, which further cluster into larger spherical structures. As observed in microscopic images shown in Figure 2, the spherical structures are in fact clusters of smaller spherical structures:

$$\mathrm{Zn(CH_3COO)_2 + HO{-}CH_2CH_2{-}OH} \longrightarrow \mathrm{Zn^{2+} \cdot {}^{-}O{-}CH_2CH_2{-}O^{-} + 2CH_3COO^{-} + 2H^{+}} \quad (1)$$

$$\frac{3}{2}\mathrm{Zn(CH_3COO)_2 + HO{-}CH_2CHOHCH_2{-}OH} \longrightarrow \frac{3}{2}\mathrm{Zn^{2+} \cdot {}^{-}O{-}CH_2CHOHCH_2{-}O^{-}} + 3\mathrm{CH_3COO^{-}} + 3\mathrm{H^{+}} \quad (2)$$

$$\mathrm{Zn(CH_3COO)_2 + HO{-}CH_2CH_2OCH_2CH_2{-}OH} \longrightarrow \mathrm{Zn^{2+} \cdot {}^{-}O{-}CH_2CH_2OCH_2CH_2{-}O^{-}} + 2\mathrm{CH_3COO^{-}} + 2\mathrm{H^{+}}. \quad (3)$$

3.4. Photocatalytic Activity Test. 4 mL of 5 ppm methylene blue solution was respectively added to 0.1 g of the three types of ZnO and commercial ZnO, followed by irradiation with 254 nm UV light. The degradation rate of ZnO fibers as the catalyst was the highest (Figure 8); after 10 minutes, the concentration of methylene blue reduced by 50%. The concentrations of the methylene blue solutions added to the ZnO sheets, ZnO spheres, and commercial ZnO were still approximately 90%. The degradation rates from the highest to the lowest were ZnO fibers > ZnO sheets > commercial ZnO > ZnO spheres.

4. Conclusion

This study employed the sol-gel method to synthesize ZnO polycrystalline nanostructures using ZnAc as the solute and various polyols as solvents (EG, G, and DEG). Zinc alkoxide crystals of varying morphologies were successfully fabricated at 160°C. The EG, G, and DEG solvents synthesized fiber-like nanostructures, rhombic flakes, and spherical particles, respectively. The surface morphology of the samples dried at 160°C was smooth. By contrast, the samples calcinated at 500°C in air gained sufficient energy to enable pyrolysis of the zinc alkoxide and sintering into the smaller ZnO molecules. Consequently, a considerable number of cracks and holes appeared, which, however, had no effect on the overall morphology. The XRD graphs and FE-TEM images mutually verify the increase in crystallinity following calcination as well as the polycrystalline structures of ZnO.

By the results, we proposed models of the relevant formation mechanisms taking into account ionic bonding and three-dimensional obstacles. A photocatalyst activity test was performed on the synthetic products and the commercial ZnO. The results indicate that the catalytic effect of ZnO fibers was the most effective.

References

[1] D. C. Look, J. W. Hemsky, and J. R. Sizelove, "Residual native shallow donor in ZnO," *Physical Review Letters*, vol. 82, no. 12, pp. 2552–2555, 1999.

[2] Y. W. Heo, D. P. Norton, L. C. Tien et al., "ZnO nanowire growth and devices," *Materials Science and Engineering R*, vol. 47, no. 1-2, pp. 1–47, 2004.

[3] K. Ellmer, "Resistivity of polycrystalline zinc oxide films: current status and physical limit," *Journal of Physics D*, vol. 34, no. 21, pp. 3097–3108, 2001.

[4] A. Ohtomo, M. Kawasaki, Y. Sakurai et al., "Fabrication of alloys and superlattices based on ZnO towards ultraviolet laser," *Materials Science and Engineering B*, vol. 56, no. 2-3, pp. 263–266, 1998.

[5] J. Wang and L. Gao, "Synthesis and characterization of ZnO nanoparticles assembled in one-dimensional order," *Inorganic Chemistry Communications*, vol. 6, no. 7, pp. 877–881, 2003.

[6] A. Kajbafvala, M. R. Shayegh, M. Mazloumi et al., "Nanostructure sword-like ZnO wires: rapid synthesis and characterization through a microwave-assisted route," *Journal of Alloys and Compounds*, vol. 469, no. 1-2, pp. 293–297, 2009.

[7] P. Li, Y. Wei, H. Liu, and X. Wang, "A simple low-temperature growth of ZnO nanowhiskers directly from aqueous solution containing $Zn(OH)_4^{2-}$ ions," *Chemical Communications*, no. 24, pp. 2856–2857, 2004.

[8] S. W. Kuo, Y. C. Chung, K. U. Jeong, and F. C. Chang, "A simple route from monomeric nanofibers to zinc oxide/zinc sulfide nanoparticle/ polymer composites through the combined use of γ-irradiation polymerization, gas/solid reaction and thermal decomposition," *Journal of Physical Chemistry C*, vol. 112, no. 42, pp. 16470–16477, 2008.

[9] C. Bae, H. Yoo, S. Kim et al., "Template-directed synthesis of oxide nanotubes: fabrication, characterization, and applications," *Chemistry of Materials*, vol. 20, no. 3, pp. 756–767, 2008.

[10] Q. Cui, K. Yu, N. Zhang, and Z. Zhu, "Porous ZnO nanobelts evolved from layered basic zinc acetate nanobelts," *Applied Surface Science*, vol. 254, no. 11, pp. 3517–3521, 2008.

[11] L. Wu, Y. Wu, and Y. Lü, "Self-assembly of small ZnO nanoparticles toward flake-like single crystals," *Materials Research Bulletin*, vol. 41, no. 1, pp. 128–133, 2006.

[12] S. -H. Yu and M. Yoshimura, "Shape and phase control of ZnS nanocrystals: template fabrication of wurtzite ZnS single-crystal nanosheets and ZnO flake-like dendrites from a lamellar molecular precursor $ZnS{\cdot}(NH_2\ CH_2\ CH_2\ NH_2)_{0.5}$," *Advanced Materials*, vol. 14, no. 4, pp. 296–300, 2002.

[13] S. Chen, Y. Liu, C. Shao et al., "Structural and optical properties of uniform ZnO nanosheets," *Advanced Materials*, vol. 17, no. 5, pp. 586–590, 2005.

[14] L. Tang, S. Yang, Y. Guo, and B. Zhou, "Building block-tunable synthesis of self-assembled ZnO quasi-microspheres via a facile liquid process," *Chemical Engineering Journal*, vol. 165, no. 1, pp. 370–377, 2010.

[15] H. Wang, K. P. Yan, J. Xie, and M. Duan, "Fabrication of ZnO colloidal photonic crystal by spin-coating method," *Materials Science in Semiconductor Processing*, vol. 11, no. 2, pp. 44–47, 2008.

[16] W. Lee, M. C. Jeong, and J. M. Myoung, "Catalyst-free growth of ZnO nanowires by metal-organic chemical vapour deposition (MOCVD) and thermal evaporation," *Acta Materialia*, vol. 52, no. 13, pp. 3949–3957, 2004.

[17] B. P. Zhang, N. T. Binh, K. Wakatsuki et al., "Pressure-dependent ZnO nanocrsytal growth in a chemical vapor deposition process," *Journal of Physical Chemistry B*, vol. 108, no. 30, pp. 10899–10902, 2004.

[18] Y. W. Wang, L. D. Zhang, G. Z. Wang, X. S. Peng, Z. Q. Chu, and C. H. Liang, "Catalytic growth of semiconducting zinc oxide nanowires and their photoluminescence properties," *Journal of Crystal Growth*, vol. 234, no. 1, pp. 171–175, 2002.

[19] M. H. Huang, Y. Wu, H. Feick, N. Tran, E. Weber, and P. Yang, "Catalytic growth of zinc oxide nanowires by vapor transport," *Advanced Materials*, vol. 13, no. 2, pp. 113–116, 2001.

[20] C. H. Liu, W. C. Yiu, F. C. K. Au, J. X. Ding, C. S. Lee, and S. T. Lee, "Electrical properties of zinc oxide nanowires and intramolecular p-n junctions," *Applied Physics Letters*, vol. 83, no. 15, pp. 3168–3170, 2003.